A Monte Carlo Exploration of Stellar Evolution and Remnants in the Milky Way

Vicente Izzo D.[1]★
[1]Departamento de Física
Universidad Técnica Federico Santa María, Av. Vicuña Mackenna 3939, 8940897 San Joaquín, Región Metropolitana, Chile

Accepted XXX. Received YYY; in original form ZZZ

ABSTRACT

We examine the distribution of stellar masses and final stellar remnants across various sample sizes to understand how stellar population characteristics evolve and compare to the observed stellar composition in the Milky Way. By analyzing samples from 100 to 1,000,000 stars, we observe that the fractions of main sequence stars, white dwarfs, neutron stars, and black holes stabilize with increasing sample size, yielding a realistic representation of stellar types. The mass distributions indicate that main sequence stars dominate the population, while white dwarfs, neutron stars, and black holes appear in decreasing frequency, consistent with initial-to-final mass relations. Age distributions further reveal the specific age ranges occupied by each stellar remnant type, with larger samples providing a closer approximation to a mature galactic population. Our results for the largest samples closely align with the stellar composition observed in the Milky Way, emphasizing the importance of large datasets in accurately simulating stellar populations. This study contributes to the understanding of galactic stellar demographics and the evolutionary dynamics of stellar populations, supporting high-fidelity stellar population synthesis for galaxies similar to the Milky Way.

Key words: stars: formation – stars: evolution – stars: black holes – stars: white dwarfs – stars: neutron – Galaxy: stellar content – Galaxy: evolution

1 INTRODUCTION

1.1 Milky Way Population

The Milky Way (MW) is composed of several distinct stellar populations that collectively offer insights into its evolutionary history. Traditionally, the MW is divided into four major components: the galactic bulge, thin disk, thick disk, and halo, each characterized by unique stellar populations with varying chemical abundances and dynamical properties (Bland-Hawthorn & Gerhard 2016). These components, when studied collectively, reveal a detailed history of galactic formation and evolution through their different stellar ages, compositions, and distributions.

The galactic halo, for instance, is known for containing some of the oldest and most metal-poor stars in the galaxy, with metallicities ranging from $-7 < [\mathrm{Fe/H}] < -0.5$ (Beers & Christlieb 2005; Helmi 2020). This suggests that the halo formed early in the galaxy's history, potentially through the accretion of smaller satellite galaxies and star clusters, evidenced by streams and other substructures (Helmi 2020). In contrast, the thin disk contains younger stars, with metallicities around solar values ($[\mathrm{Fe/H}] \approx 0$), indicating ongoing star formation and a relatively quiet merger history in recent epochs (Kilic et al. 2017). The thick disk, characterized by stars that are enriched in α-elements, provides clues to a period of rapid star formation and subsequent quenching, likely connected to significant merger events (Wallerstein 1962; Bensby et al. 2014). The bulge, being the most heterogeneous component, contains a mix of stellar populations, ranging from very metal-poor to metal-rich stars, reflecting its complex formation history through both in-situ star formation and accretion processes (McWilliam 2016; Barbuy et al. 2018).

1.2 Evolutionary Stellar Population Synthesis Model

The study of these stellar populations and their chemical and dynamical properties has led to the development of evolutionary stellar population synthesis models, which aim to replicate the observed characteristics of galaxies by modeling their stellar content over time. These models incorporate various stellar evolutionary tracks, initial mass functions (IMFs), star formation histories (SFHs), and chemical enrichment laws to predict the integrated light and spectral features of galaxies (Conroy 2013). By comparing synthetic models with observational data from surveys like Gaia, APOGEE, and GALAH, it is possible to infer the star formation and chemical enrichment history of the MW in great detail (Gaia Collaboration 2018).

A key component of these models is the Initial Mass Function (IMF), which describes the distribution of stellar masses at birth. Different IMFs have been proposed over time, with the most commonly used being the Kroupa IMF (Kroupa 2001) and the Salpeter IMF (Salpeter 1955). The Kroupa IMF is a multi-part power-law function that reflects a flatter distribution for low-mass stars and a steeper decline for high-mass stars. On the other hand, the Salpeter IMF is a simple power law, assuming a higher proportion of massive stars compared to the Kroupa IMF. These IMFs are fundamental in

★ E-mail: vicente.izzo@usm.cl

predicting the number of stars of different masses, which ultimately affects the predicted chemical evolution and luminosity of a galaxy.

Another essential element of these models is the Star Formation History (SFH), which describes the rate at which stars form over time. The SFH can vary significantly between different components of the MW. For instance, the thin disk has experienced continuous star formation over billions of years, whereas the thick disk and halo likely formed stars during shorter, more intense bursts early in the galaxy's history (Haywood et al. 2013). Different functional forms for SFHs, such as constant, exponentially declining, or burst-like models, are used to match observations to the various components of the MW (Snaith et al. 2014).

Chemical enrichment laws, which describe how the abundance of elements changes over time as successive generations of stars enrich the interstellar medium, are also key in stellar population synthesis models. These laws depend on factors such as the IMF, SFH, and the yields from supernovae and stellar winds, making them essential for understanding the chemical evolution of galaxies (Matteucci 2012).

1.3 Monte Carlo Simulation

The Monte Carlo method is a statistical approach used to solve problems that involve random sampling to obtain numerical results. It is particularly well-suited for modeling complex systems with a large number of variables and uncertainties, such as the stellar populations of a galaxy. In the context of stellar population synthesis, Monte Carlo simulations allow us to randomly generate properties of individual stars, such as their masses, ages, and metallicities, based on predetermined probability distributions like the IMF and SFH.

The main idea behind using a Monte Carlo approach is to generate a statistically representative sample of stars by drawing random values for each parameter from their respective distributions. For example, the mass of each star is drawn from an IMF, such as the Kroupa IMF, while the formation time is determined from the SFH. By simulating a large number of stars, it becomes possible to obtain a comprehensive view of the stellar content and its evolution over time, providing insights into the overall properties of the MW.

Monte Carlo simulations are advantageous because they can easily incorporate different assumptions about the underlying distributions, allowing us to explore how changes in parameters like the IMF or SFH impact the resulting stellar population. This flexibility makes Monte Carlo methods a powerful tool for testing different scenarios and comparing the results to observational data.

In this work, we will employ a Monte Carlo approach to explore the masses and ages of stars in the MW by simulating a large number of stars based on different IMFs and SFHs. This approach will allow us to estimate the distribution of stellar remnants, including white dwarfs, neutron stars, and black holes, and assess how well these models can replicate the observed properties of the MW's different components. Ultimately, our analysis aims to provide a deeper understanding of the MW's formation and evolution by comparing synthetic populations to observational data.

2 METHOD AND RESULTS

2.1 Simulating stars data with Monte Carlo

Initially, we generated multiple samples consisting of 100, 1,000, 10,000, 100,000, and 1,000,000 stars. Subsequently, we randomly assigned masses to these stars within the range of 0.08 $M_\odot$ to 100 $M_\odot$, ensuring that the distribution follows the Kroupa initial mass function (IMF). The Kroupa IMF can be described by a multi-part power-law (See Kroupa (2001) for more details), given by:

$$\xi(m) \propto m^{-\alpha_i} = m^{\gamma}, \tag{1}$$

where

$$\begin{aligned}
\alpha_0 &= 0.3 \pm 0.7, \quad 0.01 \leq \frac{m}{M_\odot} < 0.08, \\
\alpha_1 &= 1.3 \pm 0.5, \quad 0.08 \leq \frac{m}{M_\odot} < 0.50, \\
\alpha_2 &= 2.3 \pm 0.3, \quad 0.50 \leq \frac{m}{M_\odot} < 1.00, \\
\alpha_3 &= 2.3 \pm 0.7, \quad 1.00 \leq \frac{m}{M_\odot},
\end{aligned} \tag{2}$$

where $\xi(m)\mathrm{d}m$ represents the number of single stars within the mass interval m to $m + \mathrm{d}m$.

The IMF has been empirically derived by several researchers, showing that low-mass stars are formed in much greater numbers compared to high-mass stars. Consequently, this results in the formation of significantly more white dwarfs than neutron stars or black holes.

In Figure (1), the mass distribution generated according to the Kroupa IMF for each sample size is shown. It can be seen that there is a greater number of low-mass stars compared to high-mass stars, which is consistent with our expectations.

2.2 Check the main-sequence lifetime of the stars

To determine the current evolutionary stage of each star, we assigned a birth time to each star using a uniform random distribution. The lifetime of each star in the main sequence was then calculated based on its mass using the following relation:

where $t_\odot$ is the lifetime of the Sun, taken as 10^{10} years, and $T_{\mathrm{MS}}(m)$ represents the main sequence lifetime of a star of mass m. The main sequence lifetime is inversely proportional to mass, meaning more massive stars have shorter lifetimes.

The current age of each star was calculated as:

$$\mathrm{age} = 10^{10} - t_{\mathrm{birth}} \tag{3}$$

where t_{birth} is the birth time of each star, randomly assigned between 0 and 10^{10} years. We then compared the current age of each star to its main sequence lifetime $T_{\mathrm{MS}}(M)$ to determine if the star is still in the main sequence or has evolved into a stellar remnant (e.g., a white dwarf, neutron star, or black hole). The main sequence lifetime can be approximated by:

$$T_{\mathrm{MS}}(M) = \frac{t_\odot}{M^{2.5}}, \tag{4}$$

where $t_\odot = 10^{10}$ being the Sun MS lifetime. If the current age of a star exceeds its main sequence lifetime (age $> T_{\mathrm{MS}}$), the star is classified as a stellar remnant. Otherwise, it is still considered to be on the main sequence. The number of stars that are still alive and those that have become remnants were then counted for each sample size and are summarized in Table (1).

2.3 Stellar Remnants

To further classify the stellar remnants, we used the following criteria based on the mass of the star:

- Stars with a mass greater than 20 $M_\odot$ were classified as black holes.

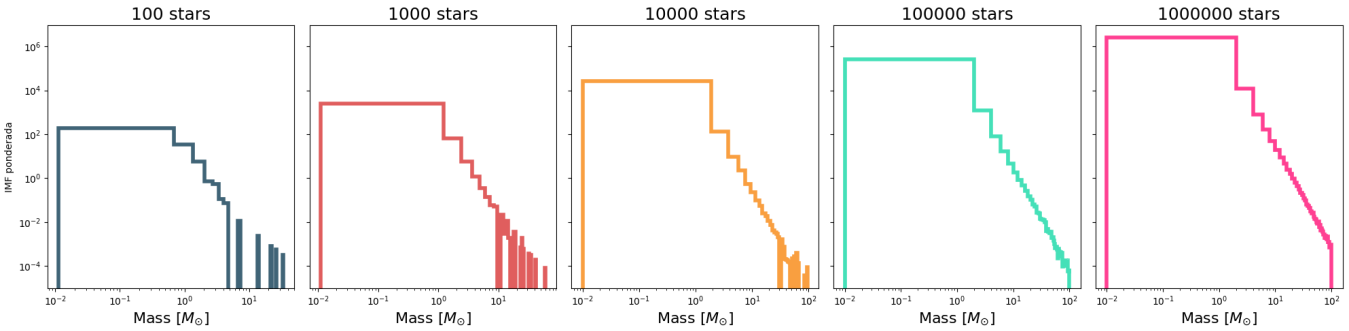

Figure 1. Mass distribution histograms for different samples of stars generated according to the Kroupa initial mass function (IMF). The panels show samples of 100, 1,000, 10,000, 100,000, and 1,000,000 stars, respectively, illustrating the predominance of low-mass stars in all sample sizes.

Sample Size	Stars in Main Sequence	Stellar Remnants
100	76	24
1,000	708	292
10,000	6,990	3,010
100,000	70,044	29,956
1,000,000	701,731	298,269

Table 1. Summary of the number of stars in the main sequence and stellar remnants for different sample sizes.

Sample Size	White Dwarf	Neutron Star	Black Hole
100	23	1	0
1,000	257	28	7
10,000	2,706	225	79
100,000	26,972	2,181	803
1,000,000	269,016	21,160	8,093

Table 2. Distribution of stellar remnants (White Dwarfs, Neutron Stars, and Black Holes) for different sample sizes.

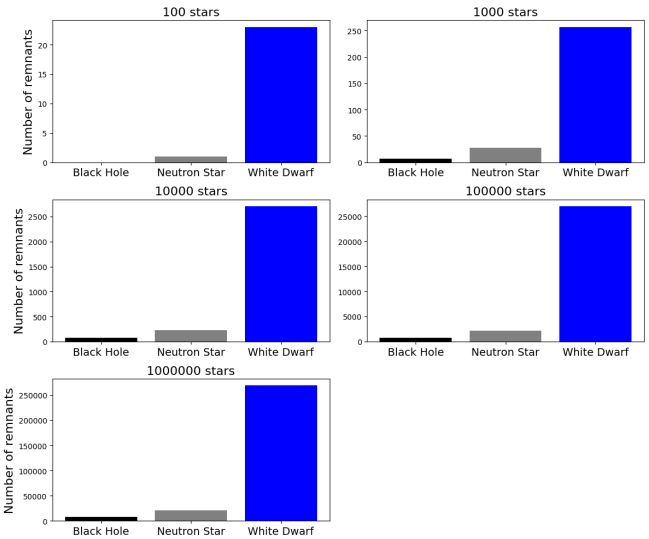

Figure 2. Classification of stellar remnants for different sample sizes generated according to the Kroupa IMF. The panels show the distribution of black holes, neutron stars, and white dwarfs for samples of 100, 1,000, 10,000, 100,000, and 1,000,000 stars. It is evident that the majority of stellar remnants are white dwarfs, while black holes and neutron stars are formed in much smaller numbers.

- Stars with a mass between 8 $M_\odot$ and 20 $M_\odot$ were classified as neutron stars.
- Stars with a mass less than 8 $M_\odot$ were classified as white dwarfs.

Using this classification, we determined the number of each type of stellar remnant in each sample. The results of this classification are shown in Figure (2) and in Table (2), which provides a breakdown of the different types of stellar remnants formed. This highlights the diversity of end states for stars depending on their initial mass.

3 ANALYSIS OF STELLAR REMNANT DISTRIBUTION

Table 2 presents the distribution of stellar remnants (White Dwarfs, Neutron Stars, and Black Holes) across varying sample sizes. As the sample size increases, a clear trend emerges in the frequency of each type of remnant. White Dwarfs are consistently the most common remnants, significantly outnumbering Neutron Stars and Black Holes. This trend is consistent with theoretical expectations, as lower-mass stars are more likely to evolve into White Dwarfs rather than Neutron Stars or Black Holes, which result from more massive progenitors.

In a sample of 100 stars, 23 White Dwarfs and only 1 Neutron Star are observed, with no Black Holes present. However, as the sample size increases to 1,000 stars, Black Holes begin to appear, and their frequency continues to rise with larger sample sizes. This increase suggests that only in larger populations can we expect to encounter the rare, massive progenitors needed for Black Hole formation.

Furthermore, the relative proportions of Neutron Stars and Black Holes remain low compared to White Dwarfs, even in the largest sample of 1,000,000 stars. White Dwarfs comprise over 90% of the remnants across all sample sizes, highlighting the predominance of lower-mass stellar evolution paths in typical stellar populations.

Overall, this distribution reflects the influence of initial stellar mass on the final remnant type, aligning with predictions from stellar evolution theory. The data underscore the rarity of massive stars capable of forming Neutron Stars and Black Holes, which explains their relatively low counts compared to White Dwarfs.

3.1 Initial-to-Final Mass Relation (IFMR) for Stellar Remnants

To estimate the final mass of stars that have evolved off the main sequence, we utilize the initial-to-final mass relation (IFMR) as implemented in SPISEA. This model maps the zero-age main-sequence (ZAMS) mass of a star to the mass and type of compact object it will become. The IFMR in SPISEA combines two widely used IFMRs: one for white dwarfs (WDs) and another for neutron stars (NSs) and black holes (BHs), as described by Hosek et al. (2020) and implemented in SPISEA (Hosek et al. (2020), section 4.3).

3.2 White Dwarf Final Mass Calculation

For white dwarfs, we employ the IFMR derived by Kalirai et al. (2008), which is based on observational data from open clusters. This relationship depends exclusively on the ZAMS mass, allowing a straightforward determination of the final WD mass. Specifically, the IFMR for white dwarfs is given by:

$$M_{\rm final} = (0.109 \pm 0.007) M_{\rm initial} + 0.394 \pm 0.025\, M_\odot \quad (5)$$

where $M_{\rm final}$ represents the final mass of the white dwarf, and $M_{\rm initial}$ is the initial mass of the star. The uncertainties in the coefficients reflect the precision of the observational fit by Kalirai et al. (2008).

3.3 Neutron Star Final Mass Calculation

For neutron star remnants, we use the IFMR derived by Raithel et al. (2018), which provides a mapping of the baryonic mass of the neutron star ($M_{\rm NS,b}$) based on the progenitor star's ZAMS mass ($M_{\rm ZAMS}$). The IFMR for neutron stars employs polynomial fits, each valid within a specific $M_{\rm ZAMS}$ range:

- For $9 \leq M_{\rm ZAMS} \leq 13\, M_\odot$, the final neutron star mass is determined by a third-order polynomial:

$$\begin{aligned} M_{\rm NS,b}(M_{\rm ZAMS}) = {} & 2.24 + 0.508(M_{\rm ZAMS} - 14.75) \\ & + 0.125(M_{\rm ZAMS} - 14.75)^2 \\ & + 0.0110(M_{\rm ZAMS} - 14.75)^3, \end{aligned} \quad (6)$$

- For $13 < M_{\rm ZAMS} < 15\, M_\odot$, a linear fit is sufficient:

$$M_{\rm NS,b}(M_{\rm ZAMS}) = 0.123 + 0.112 M_{\rm ZAMS} \quad (7)$$

- For $15 \leq M_{\rm ZAMS} < 17.8\, M_\odot$:

$$M_{\rm NS,b}(M_{\rm ZAMS}) = 0.996 + 0.0384 M_{\rm ZAMS} \quad (8)$$

- For $17.8 < M_{\rm ZAMS} < 18.5\, M_\odot$:

$$M_{\rm NS,b}(M_{\rm ZAMS}) = -0.020 + 0.10 M_{\rm ZAMS} \quad (9)$$

These segmented polynomial and linear fits account for variations in stellar evolution across different mass regimes, providing a refined estimate of neutron star masses.

3.4 Black Hole Final Mass Calculation

For black holes, we use the IFMR provided by Raithel et al. (2018), which differentiates between various ZAMS mass ranges. The final black hole mass depends on whether only the He-core collapses or the entire star does, as detailed below:

- For $15 \leq M_{\rm ZAMS} < 40\, M_\odot$, in scenarios where only the He-core collapses ($f_{\rm ej} = 0$):

$$M_{\rm BH,core}(M_{\rm ZAMS}) = -2.049 + 0.4140 M_{\rm ZAMS} \quad (10)$$

- For $15 \leq M_{\rm ZAMS} < 40\, M_\odot$, when the entire star collapses ($f_{\rm ej} = 0$):

$$\begin{aligned} M_{\rm BH,all}(M_{\rm ZAMS}) = {} & 15.52 - 0.3294(M_{\rm ZAMS} - 25.97) \\ & + 0.02121(M_{\rm ZAMS} - 25.97)^2 \\ & + 0.003120(M_{\rm ZAMS} - 25.97)^3 \end{aligned} \quad (11)$$

- For $45 \leq M_{\rm ZAMS} < 120\, M_\odot$, where only the CO-core collapses:

$$M_{\rm BH,core}(M_{\rm ZAMS}) = 5.697 + 7.8598 \times 10^8 (M_{\rm ZAMS})^{-4.858} \quad (12)$$

The final black hole mass can also be expressed as a combination of $M_{\rm BH,core}$ and $M_{\rm BH,all}$, with an ejection fraction $f_{\rm ej}$ defining the amount of material ejected:

$$M_{\rm BH}(M_{\rm ZAMS}; f_{\rm ej}) = f_{\rm ej} M_{\rm BH,core}(M_{\rm ZAMS}) + (1 - f_{\rm ej}) M_{\rm BH,all}(M_{\rm ZAMS}) \quad (13)$$

This framework allows for various collapse scenarios, depending on progenitor mass and dynamics, enabling accurate predictions of black hole masses.

In Figure 3, we present the final mass distributions for each type of stellar remnant—black holes, neutron stars, and white dwarfs—as well as main sequence stars, across different sample sizes. This figure allows us to examine how the distribution of final masses varies depending on the type of remnant and the total number of stars in the sample.

From the figure, we observe distinct trends in the mass distributions for each type of remnant. The main sequence stars (teal) exhibit a broader mass range that decreases in probability density as we move towards higher masses, consistent with the initial mass function's steep slope. Black holes (yellow) tend to populate the higher mass end, showing a relatively stable distribution as the sample size increases. Neutron stars (red) appear as narrower, more concentrated distributions at intermediate masses, reflecting the limited mass range that leads to neutron star formation. White dwarfs (purple), on the other hand, show a mass distribution peaking at lower values, which aligns with the expected outcomes of lower-mass progenitors.

As the sample size increases, we can also see an overall increase in the stability and clarity of the distributions for each remnant type. In smaller samples (e.g., 100 or 1,000 stars), statistical noise introduces more variability in the histograms. However, as the sample size reaches 100,000 or 1,000,000 stars, the distributions become smoother and more defined, accurately representing the underlying initial-to-final mass relations (IFMR) used in the simulation.

The logarithmic scale on the y-axis highlights the variation in probability density across the different populations. Notably, black holes and neutron stars are present at lower densities compared to main sequence stars and white dwarfs, emphasizing their relative rarity in typical stellar populations. This variation underscores the importance of sample size when studying the statistical properties of stellar remnants.

Figure 3 presents the age distribution of various types of stellar objects—main sequence stars, black holes, neutron stars, and white dwarfs—across different sample sizes (100, 1,000, 10,000, 100,000, and 1,000,000 stars). This figure provides insight into the evolution of stellar populations over time and allows us to examine how each type's prevalence changes as we increase the sample size.

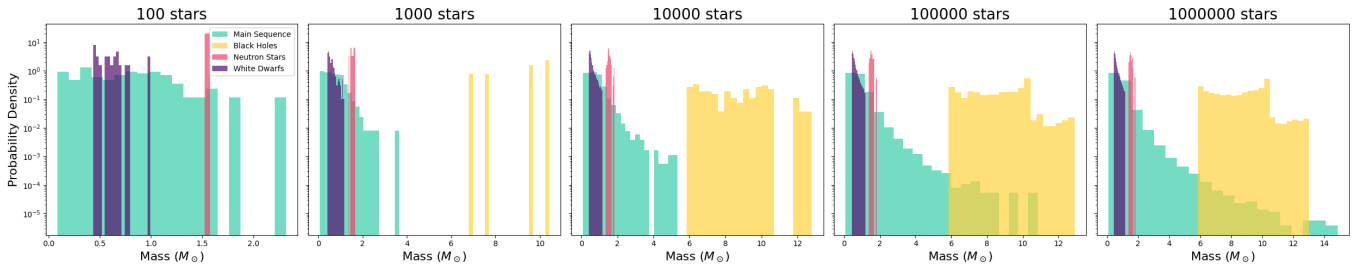

Figure 3. Probability density distribution of masses for different types of stellar remnants and main sequence stars, shown for sample sizes of 100, 1,000, 10,000, 100,000, and 1,000,000 stars. Each subplot displays density histograms for main sequence stars (teal), black holes (yellow), neutron stars (red), and white dwarfs (purple). The y-axis is in logarithmic scale to highlight the variation in probability density across the different populations of remnants and stars.

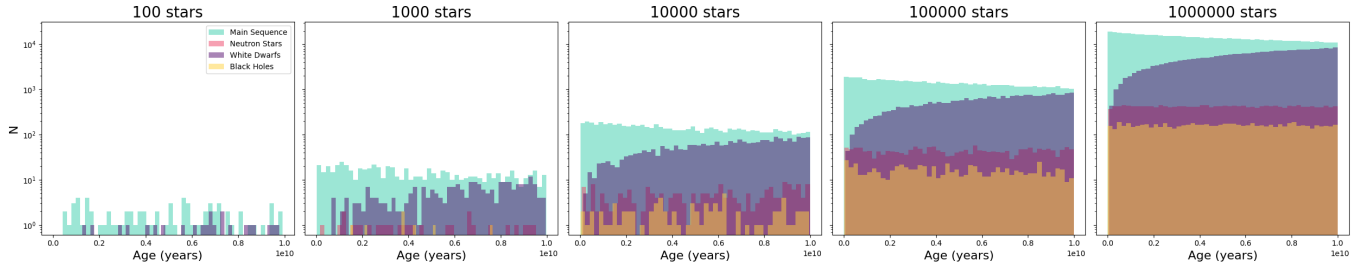

Figure 4. Age distribution of different types of stellar objects for various sample sizes (100, 1,000, 10,000, 100,000, and 1,000,000 stars). Each subplot shows histograms of ages for main sequence stars (teal), black holes (yellow), neutron stars (red), and white dwarfs (purple). The logarithmic scale on the y-axis highlights the variation in counts across different ages and stellar types, with larger samples providing a clearer and more stable distribution pattern. This figure illustrates how the relative population of each type evolves over time, with a notable increase in the main sequence population across all sample sizes.

In the smaller sample sizes (100 and 1,000 stars), the distributions exhibit more variability and noise, making it challenging to discern clear patterns. As the sample size grows to 10,000 stars and beyond, the distributions stabilize, offering a more robust representation of each population's age distribution. This effect is particularly evident in the larger samples, where main sequence stars (teal) dominate across all ages, while the other stellar remnants—black holes (yellow), neutron stars (red), and white dwarfs (purple)—appear in relatively lower numbers.

The logarithmic scale on the y-axis reveals significant differences in population counts between main sequence stars and stellar remnants. Main sequence stars consistently show the highest counts, which decrease gradually with age, reflecting a continuous supply of younger stars. White dwarfs and neutron stars display more clustered age distributions, suggesting they form within a specific age range as they evolve from their progenitor stars. Black holes, while rare in comparison, appear with relatively consistent numbers across ages, indicative of the limited range of progenitor stars that undergo collapse to form black holes.

Overall, this figure illustrates that as the sample size increases, the distribution patterns of stellar ages become more defined. Larger samples allow for a clearer observation of the evolutionary timeline of stellar populations, showing how different types of stellar remnants populate specific age ranges within the overall population. This trend highlights the importance of large datasets in stellar population studies to achieve statistically significant insights into the age distributions and evolutionary pathways of various types of stellar objects.

Table 3 shows the fractions of each stellar population type—main sequence stars (MS), white dwarfs (WD), neutron stars (NS), and black holes (BH)—across different sample sizes. These results offer insights into how the composition of a simulated stellar population stabilizes with larger sample sizes, facilitating a direct comparison with observed fractions in the Milky Way.

Sample Size	MS	WD	NS	BH
100	0.76	0.23	0.01	0.00
1,000	0.708	0.257	0.028	0.007
10,000	0.699	0.2706	0.0225	0.0079
100,000	0.70044	0.26972	0.02181	0.00803
1,000,000	0.701731	0.269016	0.02116	0.008093

Table 3. Fraction of each stellar population type for different sample sizes.

As indicated in the table, the fraction of main sequence stars (MS) decreases slightly from 0.76 in the smallest sample size (100 stars) to around 0.70 in the largest sample sizes. This decline reflects the fact that in larger, older stellar populations, a higher proportion of stars have evolved off the main sequence. This is consistent with observed trends in the Milky Way, where a similar decrease is seen as stars age and evolve, supported by population synthesis models and observational data (Kalirai 2008; Cummings & Kalirai 2018).

For white dwarfs (WD), the fraction rises from 0.23 to approximately 0.27 as the sample size increases. This trend aligns with expectations, as a large fraction of low- to intermediate-mass stars, which are prevalent in the Milky Way, end their life cycles as white dwarfs. Studies suggest that white dwarfs account for around 97% of

post-main-sequence stars, confirming the importance of white dwarfs in remnant populations (Kalirai 2008; Cummings & Kalirai 2018).

The fractions of neutron stars (NS) and black holes (BH) remain relatively low across all sample sizes, which is consistent with the relatively rare occurrence of high-mass progenitors capable of evolving into these compact objects. In larger samples, the neutron star fraction stabilizes around 0.021, while black holes maintain a fraction close to 0.008. These values align with Milky Way estimates, where neutron stars and black holes constitute a small fraction of the total stellar population due to the specific, high-mass progenitors required for their formation (Lorimer 2006; Fryer 2012).

In conclusion, as sample sizes grow, the fractions of each stellar type become more consistent and reflective of the Milky Way's composition. This suggests that large sample sizes are crucial for accurately simulating stellar remnant distributions in galaxies and for making meaningful comparisons with observed galactic populations.

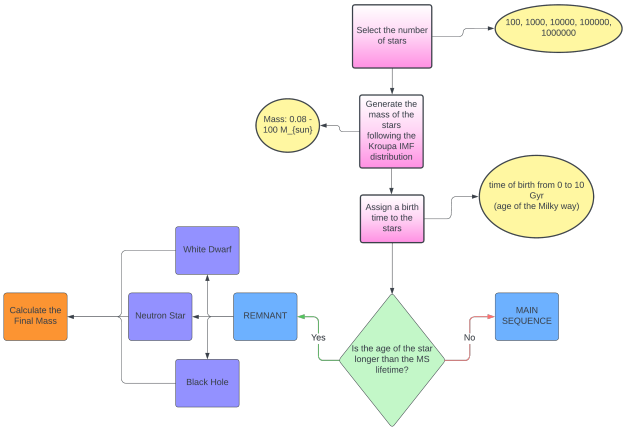

Figure 5. Flowchart of the simulation process for generating and classifying stellar populations. The flowchart outlines the steps for selecting the number of stars, assigning masses following the Kroupa IMF, determining birth times, and classifying stars as either main sequence or different types of stellar remnants (white dwarfs, neutron stars, or black holes).

4 CONCLUSIONS

In this study, we examined the distribution of stellar masses and final stellar remnants across various sample sizes, aiming to understand how stellar population characteristics evolve and how they compare to the observed stellar composition in the Milky Way. Our analysis revealed several key insights:

(i) **Stabilization of Stellar Fractions with Sample Size**: As the sample size increased, the fractions of main sequence stars, white dwarfs, neutron stars, and black holes reached stable values, reflecting a realistic distribution of stellar types. Smaller sample sizes showed higher variability and noise, while larger samples (100,000 and 1,000,000 stars) provided more accurate representations of stellar populations, closely aligning with expected galactic proportions.

(ii) **Distribution of Stellar Remnant Types**: The mass distributions demonstrated that main sequence stars constitute the largest fraction of the stellar population, with a decreasing probability density as mass increases. White dwarfs formed a significant fraction among stellar remnants, particularly at lower masses, while neutron stars and black holes appeared at relatively low frequencies, consistent with their formation from high-mass progenitors. These findings align with expectations based on initial-to-final mass relations (IFMR) and support observations of remnant populations in the Milky Way.

(iii) **Age Distribution and Evolution of Stellar Types**: The age distributions for each type of stellar object, visualized across sample sizes, revealed how different types of stellar remnants populate specific age ranges. Main sequence stars dominated across all ages, while white dwarfs, neutron stars, and black holes were distributed within narrower age bands, reflecting the evolutionary pathways of their progenitors. As sample size increased, the age distributions became smoother and more representative of an actual galactic stellar population.

(iv) **Comparison with the Milky Way's Stellar Composition**: The fractions obtained for each stellar type in the largest samples showed a close resemblance to the stellar composition observed in the Milky Way. In particular, the main sequence stars in our model comprise approximately 70% of the total population, white dwarfs approximately 27%, neutron stars around 2.1%, and black holes near 0.8%. These proportions align with estimates for the Milky Way's stellar population, where main sequence stars and white dwarfs dominate, and neutron stars and black holes constitute smaller fractions due to the necessity of high-mass progenitors for their formation (Kalirai 2008; Cummings & Kalirai 2018; Lorimer 2006; Fryer 2012).

In conclusion, this study highlights the importance of large sample sizes in simulating stellar populations, as they enable more precise modeling of the distribution of stellar remnants and provide a reliable basis for comparison with observed galactic populations. These findings underscore the value of high-fidelity stellar population synthesis in understanding the evolutionary dynamics and composition of galaxies similar to the Milky Way.

DATA AVAILABILITY

The code used for this simulation, including data generation and analysis, is publicly available at the following link: GitHub Repository. This repository contains both the source code in Jupyter Notebook format and detailed instructions for execution. Open access is permitted for verification and reproducibility purposes.

REFERENCES

Barbuy B., Chiappini C., Gerhard O., 2018, Annual Review of Astronomy and Astrophysics, 56, 223–276
Beers T. C., Christlieb N., 2005, ARA&A, 43, 531
Bensby T., Feltzing S., Oey M. S., 2014, A&A, 562, A71
Bland-Hawthorn J., Gerhard O., 2016, ARA&A, 54, 529
Conroy C., 2013, ARA&A, 51, 393
Cummings J. D., Kalirai J. S. e. a., 2018, Monthly Notices of the Royal Astronomical Society, 473, 1186
Fryer C. L. e. a., 2012, The Astrophysical Journal, 749, 91
Gaia Collaboration 2018, VizieR Online Data Catalog: Gaia DR2 (Gaia Collaboration, 2018), VizieR On-line Data Catalog: I/345. Originally published in: 2018A&A...616A...1G; doi:10.5270/esa-ycs, doi:10.26093/cds/vizier.1345
Haywood M., Di Matteo P., Lehnert M. D., Katz D., Gómez A., 2013, Astronomy & Astrophysics, 560, A109
Helmi A., 2020, ARA&A, 58, 205
Hosek Matthew W. J., Lu J. R., Lam C. Y., Gautam A. K., Lockhart K. E., Kim D., Jia S., 2020, AJ, 160, 143

Kalirai J. S. e. a., 2008, The Astrophysical Journal, 676, 594
Kalirai J. S., Hansen B. M. S., Kelson D. D., Reitzel D. B., Rich R. M., Richer H. B., 2008, ApJ, 676, 594
Kilic M., Munn J. A., Harris H. C., von Hippel T., Liebert J. W., Williams K. A., Jeffery E., DeGennaro S., 2017, ApJ, 837, 162
Kroupa P., 2001, MNRAS, 322, 231
Lorimer D. R. e. a., 2006, Monthly Notices of the Royal Astronomical Society, 372, 777
Matteucci F., 2012, Chemical Evolution of Galaxies, doi:10.1007/978-3-642-22491-1.
McWilliam A., 2016, Publ. Astron. Soc. Australia, 33, e040
Raithel C. A., Sukhbold T., Özel F., 2018, ApJ, 856, 35
Salpeter E. E., 1955, ApJ, 121, 161
Snaith O. N., Haywood M., Di Matteo P., Lehnert M. D., Combes F., Katz D., Gómez A., 2014, ApJ, 781, L31
Wallerstein G., 1962, ApJS, 6, 407

This paper has been typeset from a TEX/LATEX file prepared by the author.